A Framework for Uplink ISAC Receiver Designs: Performance Analysis and Algorithm Development

Zhiyuan Yu, Hong Ren, *Member, IEEE*, Cunhua Pan, *Senior Member, IEEE*, Gui Zhou, *Member, IEEE*, Dongming Wang, *Member, IEEE*, Chau Yuen, *Fellow, IEEE*, Jiangzhou Wang, *Fellow, IEEE*,

Abstract—Uplink integrated sensing and communication (ISAC) systems have recently emerged as a promising research direction, enabling simultaneous uplink signal detection and target sensing. In this paper, we propose flexible projection (FP)-type receivers that unify the projection-type receivers and the successive interference cancellation (SIC)-type receivers by using a flexible tradeoff factor to adapt to dynamically changing uplink ISAC scenarios. The FP-type receivers address the joint signal detection and target response estimation problem through two coordinated phases: 1) Communication signal detection using a reconstructed signal whose composition is controlled by the tradeoff factor, followed by 2) Target response estimation performed through subtraction of the detected communication signal from the received signal. With adjustable tradeoff factors, the FP-type receivers can balance the enhancement of the signal-to-interference-plus-noise ratio (SINR) with the reduction of correlation in the reconstructed signal for communication signal detection. The pairwise error probabilities (PEPs) are analyzed for both maximum likelihood (ML) and zero-forcing (ZF) detectors, revealing that the optimal tradeoff factor should be determined based on the adopted detection algorithm and the relative power of the sensing and communication (S&C) signal. A homotopy optimization framework is first applied for the FP-type receivers with a fixed trade-off factor. This framework is then extended to develop dynamic FP (DFP)-type receivers, which iteratively adjust the trade-off factor for improved algorithm performance and environmental adaptability. Subsequently, two extensions are explored to further enhance the receivers' performance: parallel DFP (PDFP)-type receivers and a block-structured receiver design. Finally, the effectiveness of the proposed receiver designs is verified via simulations.

Index Terms—Integrated sensing and communication (ISAC), receiver designs.

I. INTRODUCTION

Low-altitude economy (LAE) is anticipated to facilitate a variety of applications in transportation, environmental monitoring, agriculture, and entertainment, generating significant economic and social value. Integrated sensing and communications (ISAC) [1], [2], a key technology for sixth-generation (6G) wireless networks, has emerged as an effective solution to support LAE [3], [4]. The continuous development of ISAC enables base stations (BSs) to communicate with designated

Part of our work has been accepted by ICC 2025. Zhiyuan Yu, Hong Ren, Cunhua Pan, Dongming Wang, and Jiangzhou Wang are with National Mobile Communications Research Laboratory, Southeast University, Nanjing, China. (e-mail:{zyyu, hren, cpan, wangdm, j.z.wang}@seu.edu.cn). Gui Zhou is with the Institute for Digital Communications from Friedrich-Alexander Universität of Erlangen-Nüremberg (FAU), Erlangen, Germany. (email: gui.zhou@fau.de). Chau Yuen is with the School of Electrical and Electronics Engineering, Nanyang Technological University, Singapore 639798. (e-mail:chau.yuen@ntu.edu.sg).

(*Corresponding authors: Hong Ren and Cunhua Pan.*)

UAVs while simultaneously sensing the location and velocity of other aerial targets, thereby establishing dual-functional capabilities for heterogeneous service demands. This dual-functional integration demonstrates particular advantages in enhancing operational efficiency and safety assurance for latency-sensitive applications such as real-time logistics tracking and aerial surveillance systems.

In contrast to traditional terrestrial networks that primarily emphasize downlink services, UAVs require sustained uplink transmission for multi-modal sensing data, such as video streams, and environmental sampling data, leading to higher uplink data rate demands. The coexistence of these uplink-dominated communication services with the continuous sensing requirements for targets presents substantial challenges for future ISAC networks. Although these sensing and communication (S&C) services can be supported by using different subcarrier or time resource blocks, this leads to low resource utilization. To better exploit spectrum resources for enhanced S&C performance, particularly for continuous sensing, uplink ISAC receivers are expected to detect uplink communication signal and simultaneously estimate target-related parameters from the echoes. However, these concurrent S&C tasks introduce significant mutual interference, making receiver designs for uplink ISAC systems both intriguing and challenging.

Several initial investigations have been conducted in uplink ISAC systems, focusing on systems architecture design [5], [6], performance analysis [7]–[10], and transceiver beamforming [11]–[13]. These architecture designs explored the potential of uplink ISAC systems and offered an initial attempt at addressing the challenging joint signal detection and sensing estimation problem. The contributions in performance analysis mainly aim to derive analytical results for the outage probability, sensing rate, and their asymptotic performance. These studies indicated that, despite mutual interference, ISAC receivers can offer increased degrees of freedom (DoFs) for both S&C functionalities compared to frequency-division S&C systems. Meanwhile, several contributions focused on transceiver design in uplink ISAC, exploring the S&C performance tradeoff and interference mitigation through power allocation and beamforming techniques.

All the aforementioned research primarily focused on exploring the potential of uplink ISAC systems with successive interference cancellation (SIC)-type receivers. Notably, in studies on architecture design [5], [6], communication signal detection and radar target estimation were performed sequentially. Furthermore, performance metrics used in analyses and transceiver beamforming, such as sensing rate [7]

and communication and sensing SINR [12], were derived by treating the mutual interference as noise, which is a key characteristic of SIC-type receivers. However, SIC-type receivers represent a heuristic approach to the joint signal detection and sensing problem and have been shown to be suboptimal in simplified system setups [14]. Furthermore, the use of SIC-type receivers necessitates a significant power difference between S&C signals, which cannot be used in the case where the powers of communication and sensing signal are comparable.

To further harness the potential of uplink ISAC systems, it is crucial to design more efficient receivers to mitigate mutual interference or, equivalently, solve the joint uplink communication signal detection and target response estimation problem. Although the considered joint problem looks similar to some problems including joint channel estimation and signal detection [15], and interference elimination in the radar-communication coexistence (RCC) systems [16], [17], their objectives and design principles differ fundamentally. Specifically, in the joint channel estimation and signal detection problems, a turbo-like structure was employed where channel estimation and signal detection were iteratively refined, using data to enhance channel estimation accuracy. In the RCC systems, the receivers were designed by exploiting the frequency sparsity to suppress radar interference for communication signal detection [16], or vice versa [17].

More relevant to this study, the joint communication signal detection and target estimation problem was investigated and the projection-type receivers for uplink ISAC systems were proposed in [18]. In [18], the joint communication signal detection and target estimation problem was transformed into an equivalent two-step problem by projection. Specifically, the communication signal was detected in a transformed signal detection problem and the sensing estimation was performed after the communication symbols were detected. Unlike SIC-type receivers, which treat mutual interference as noise, projection-type receivers fully eliminated the sensing interference during communication signal detection, making it possible to achieve high S&C performance simultaneously. However, the projection-type receivers still face several implementation challenges, such as rank deficiency and high computational complexity introduced by joint estimation of the communication signal across multiple snapshots. Furthermore, two fundamental problems remain unaddressed in uplink ISAC receiver designs: **(1)** Directly applying existing multiple-input multiple-output (MIMO) signal detection algorithms to the transformed communication signal detection problem either suffers from high computational complexity or poor performance when rank deficiency occurs. How can uplink ISAC receivers be designed with tailored low-complexity algorithms that provide performance guarantees? **(2)** The power of the S&C signal directly influences the strength of mutual interference, necessitating the use of different receiver types to achieve optimal performance. However, the received power of the sensing signal is determined by the environment and the movement of the target, which may change rapidly and is not known to the receiver. In this case, is it possible to develop environment-adaptive receivers that can operate effectively with varying S&C power?

Against the above background, our contributions are summarized as follows:

1) The joint signal detection and target response estimation problem in uplink ISAC systems is investigated, and a general framework called flexible projection (FP)-type receivers with a tradeoff factor is introduced. In the proposed FP-type receivers, the communication signal is detected using a reconstructed signal formed by combining two signal components of the received signal: one from the complement space of the radar waveform and the other from the signal space of the radar waveform, where the tradeoff factor controls the ratio of the signal space component. Then, the FP-type receivers perform the target response estimation by subtracting the estimated communication signal from the received signal.

2) We show that decreasing the tradeoff factor increases the signal-to-interference-plus-noise ratio (SINR) of the signal detection problem but also amplifies the undesired correlation between the received signals. Then, the pairwise error probabilities (PEPs) of the FP-type receivers are studied for the maximum likelihood (ML) detector and zero-forcing (ZF) detector, respectively. The derived results reveal that the optimal tradeoff factor is determined according to the communication signal detection algorithm as well as the power of the S&C signal and the noise.

3) Building upon a MIMO signal detection algorithm using homotopy optimization, we propose the dynamic FP (DFP)-type receivers. The proposed algorithm transforms the formulated signal detection problem into a continuous optimization problem. By adjusting the tradeoff factor in each iteration, the DFP-type receivers provide a smoother approximation to the original joint signal detection and target estimation problem and offer superior environmental adaptability compared to the traditional FP-type receivers.

4) Finally, two extensions are discussed to enhance the performance of the uplink ISAC receivers. The first is the parallel DFP (PDFP)-type receivers, which employ multiple DFP-type receivers to further improve their environmental adaptability. The second extension involves the block structure of the uplink ISAC receivers, which uses prior information about the target to enhance the receivers' performance.

The remainder of this paper is organized as follows. In Section II, we present the system model and review the SIC-type receivers and projection-type receivers. A general receiver design principle and corresponding performance evaluation is presented in Section III. A low complexity algorithm is developed in Section IV. In Section V, two algorithm extensions are discussed. Finally, Sections VI and VII show the numerical results, and conclusions, respectively.

Notations: $\mathbb{C}^{M \times N}$ denotes the set of $M \times N$ complex matrices. $\mathbb{E}[\cdot]$ denotes the expectation operation. $\|\mathbf{x}\|_2$ denotes the 2-norm of vector $\mathbf{x}$. $\mathbf{X} \otimes \mathbf{Y}$ denotes the Kronecker
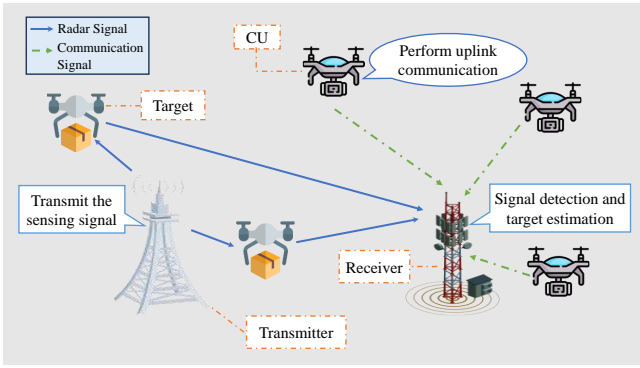
Fig. 1: Considered uplink ISAC systems

Fig. 2: Various types of receiver designs in uplink ISAC systems

product between $\mathbf{X}$ and $\mathbf{Y}$. $\mathrm{Rank}(\mathbf{X})$, $\|\mathbf{X}\|_F$, $\|\mathbf{X}\|_2$, $\mathrm{vec}(\mathbf{X})$, $\mathrm{Tr}(\mathbf{X})$, $\lambda_i(\mathbf{X})$, $\omega_j(\mathbf{X})$ denote the rank, Frobenius norm, spectrum norm, vectorization operation, trace operation, the i-th largest eigenvalue and the j-th largest singular value of $\mathbf{X}$, respectively. $\mathbf{I}_N$ denotes the $N \times N$ identity matrix. $\mathcal{CN}(\mathbf{0}, \mathbf{I})$ represents a circularly symmetric complex Gaussian random vector with zero mean and unit variance matrix. $(\cdot)^{\mathrm{T}}$, $(\cdot)^*$, $(\cdot)^{\mathrm{H}}$, $(\cdot)^{-1}$, and $(\cdot)^{\dagger}$ denote the transpose, conjugate, Hermitian, inverse, and pseudoinverse operators, respectively. The convex hull of a non-empty set $\mathcal{X}$ is denoted by $\mathrm{conv}(\mathcal{X})$.

II. REVIEW OF UPLINK ISAC RECEIVER DESIGNS

A. System Model

We consider an uplink MIMO ISAC system shown in Fig. 1, consisting of K single-antenna communication users (CUs) and multiple targets. We assume that a transmitter equipped with M_t transmit antennas is used to transmit the sensing signal, and a receiver equipped with M_r receive antennas receives both the uplink communication signal and the radar echo, where $K \leq M_r$.

The target sensing is implemented over a coherent processing interval consisting of L snapshots. The transmitted sensing signal at the transmitter at the l-th snapshot, $\mathbf{x}_{\mathrm{r}}[l] \in \mathbb{C}^{M_t \times 1}$, satisfies $\mathbb{E}[\mathbf{x}_{\mathrm{r}}[l]] = \mathbf{0}$ and $\mathbb{E}[\mathrm{Tr}(\mathbf{x}_{\mathrm{r}}[l]\mathbf{x}_{\mathrm{r}}^{\mathrm{H}}[l])] = \mathrm{Tr}(\mathbf{R}) \leq P_{\mathrm{r}}$, where $\mathbf{R} \succeq 0$ and P_{r} denote the covariance matrix and the maximum transmit power of the sensing signal, respectively. The target response matrix is denoted by $\mathbf{H}_{\mathrm{r}} \in \mathbb{C}^{M_r \times M_t}$, which contains the velocity and position of the targets. These parameters can be determined using parameter estimation methods, if the target response matrix estimation is available [19]. Denoting $\mathbf{X}_{\mathrm{r}} = [\mathbf{x}_{\mathrm{r}}[1], \cdots, \mathbf{x}_{\mathrm{r}}[L]] \in \mathbb{C}^{M_t \times L}$, the average power of the received sensing signal across L snapshots is given by $P_{\mathrm{s}} \triangleq \mathbb{E}[\|\mathbf{H}_{\mathrm{r}}\mathbf{X}_{\mathrm{r}}\|_F^2]/L$.

In each snapshot, the k-th CU transmits a modulated symbol $\tilde{x}_{\mathrm{c},k} \in \mathcal{X}$ to the receivers for uplink communication. We assume that the transmitted symbols of K CUs, $\tilde{\mathbf{x}}_{\mathrm{c},k} = [\tilde{x}_{\mathrm{c},1}, \cdots, \tilde{x}_{\mathrm{c},K}]$, are mutually uncorrelated and satisfy $\mathbb{E}[\tilde{\mathbf{x}}_{\mathrm{c},k}] = \mathbf{0}$ and $\mathbb{E}[\tilde{\mathbf{x}}_{\mathrm{c},k}\tilde{\mathbf{x}}_{\mathrm{c},k}^{\mathrm{H}}] = P_{\mathrm{c}}\mathbf{I}_M$, where P_{c} denotes the transmit power of the communication signal. We also assume that the channel state information (CSI) of the CU-receiver channel $\mathbf{H}_{\mathrm{c}}$ is perfectly known at the receiver. Due to the rich scattering environment, the channel matrix $\mathbf{H}_{\mathrm{c}}$ has full rank, i.e., $\mathrm{Rank}(\mathbf{H}_{\mathrm{c}}) = K$, and the channel matrix is normalized so that $\mathbb{E}[\|\mathbf{H}_{\mathrm{c}}\|_F^2] = KM_r$.

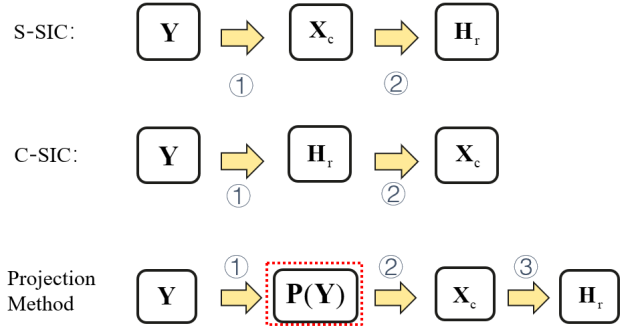We assume that the frequencies of the uplink communication signal and sensing signal are the same, then, the received signal at the l-th snapshot, $\tilde{\mathbf{y}}[l] \in \mathbb{C}^{M_r \times 1}$, is a combination of the uplink communication signal and sensing echo, given by

$$\tilde{\mathbf{y}}[l] = \underbrace{\mathbf{H}_{\mathrm{c}}\tilde{\mathbf{x}}_{\mathrm{c}}[l]}_{\text{Uplink signal}} + \underbrace{\mathbf{H}_{\mathrm{r}}\mathbf{x}_{\mathrm{r}}[l]}_{\text{Sensing echo}} + \tilde{\mathbf{n}}[l], \tag{1}$$

where $\tilde{\mathbf{n}}[l]$ denotes the additive white Gaussian noise (AWGN) at the receiver following the distribution of $\tilde{\mathbf{n}}[l] \sim \mathcal{CN}(\mathbf{0}, \sigma^2\mathbf{I}_{M_r})$ with the noise power of σ^2.

By stacking $L > M_t$ snapshots together, the received signal at the receiver can be formulated as

$$\mathbf{Y} = \mathbf{H}_{\mathrm{r}}\mathbf{X}_{\mathrm{r}} + \mathbf{H}_{\mathrm{c}}\mathbf{X}_{\mathrm{c}} + \tilde{\mathbf{N}}, \tag{2}$$

where $\mathbf{X}_{\mathrm{c}} = [\tilde{\mathbf{x}}_{\mathrm{c}}[1], \cdots, \tilde{\mathbf{x}}_{\mathrm{c}}[L]] \in \mathbb{C}^{K \times L}$, $\mathbf{Y} = [\tilde{\mathbf{y}}[1], \cdots, \tilde{\mathbf{y}}[L]] \in \mathbb{C}^{M_r \times L}$, and $\tilde{\mathbf{N}} = [\tilde{\mathbf{n}}[1], \cdots, \tilde{\mathbf{n}}[L]] \in \mathbb{C}^{M_r \times L}$.

In the considered uplink ISAC systems, receivers are responsible for simultaneously extracting the target response matrix and decoding the communication signal. Since the AWGN at the receiver follows the distribution of $\mathrm{vec}(\tilde{\mathbf{N}}) \sim \mathcal{CN}(\mathbf{0}, L\sigma^2\mathbf{I}_{M_r})$, the probability density function of $\mathbf{Y}$ given $\mathbf{X}_{\mathrm{c}}$ and $\mathbf{H}_{\mathrm{r}}$ is

$$p(\mathbf{Y} \mid \mathbf{X}_{\mathrm{c}}, \mathbf{H}_{\mathrm{r}}) = \frac{1}{(\pi L\sigma^2)^{M_r}} e^{\frac{-\|\mathbf{Y} - \mathbf{H}_{\mathrm{r}}\mathbf{X}_{\mathrm{r}} - \mathbf{H}_{\mathrm{c}}\mathbf{X}_{\mathrm{c}}\|_F^2}{L\sigma^2}}. \tag{3}$$

Thus, the maximum likelihood (ML) estimation can be formulated as a mixed integer least square (LS) problem

$$\underset{\mathbf{H}_{\mathrm{r}}, \mathbf{X}_{\mathrm{c}} \in \mathcal{X}^{K \times L}}{\arg\min} \|\mathbf{Y} - \mathbf{H}_{\mathrm{r}}\mathbf{X}_{\mathrm{r}} - \mathbf{H}_{\mathrm{c}}\mathbf{X}_{\mathrm{c}}\|_F^2. \tag{4}$$

According to the equality $\mathrm{vec}(\mathbf{A}\mathbf{C}) = (\mathbf{I} \otimes \mathbf{A})\mathrm{vec}(\mathbf{C}) = (\mathbf{C}^{\mathrm{T}} \otimes \mathbf{I})\mathrm{vec}(\mathbf{A})$ [20], (4) can be reformulated as

$$\underset{\mathbf{h}_{\mathrm{r}}, \mathbf{x}_{\mathrm{c}} \in \mathcal{X}^{LK}}{\arg\min} \|\mathbf{y} - \mathbf{A}_{\mathrm{c}}\mathbf{x}_{\mathrm{c}} - \mathbf{A}_{\mathrm{r}}\mathbf{h}_{\mathrm{r}}\|_2^2, \tag{5}$$

where $\mathbf{x}_{\mathrm{c}} = \mathrm{vec}(\mathbf{X}_{\mathrm{c}}) \in \mathbb{C}^{LK \times 1}$, $\mathbf{y} = \mathrm{vec}(\mathbf{Y}) \in \mathbb{C}^{LM_r \times 1}$, $\mathbf{A}_{\mathrm{r}} = \mathbf{X}_{\mathrm{r}}^{\mathrm{T}} \otimes \mathbf{I}_{M_r} \in \mathbb{C}^{LM_r \times M_r M_t}$, $\mathbf{A}_{\mathrm{c}} = \mathbf{I}_L \otimes \mathbf{H}_{\mathrm{c}} \in \mathbb{C}^{LM_r \times LK}$, and the target response vector is given by $\mathbf{h}_{\mathrm{r}} = \mathrm{vec}(\mathbf{H}_{\mathrm{r}}) \in \mathbb{C}^{M_r M_t \times 1}$.

Remark 1: Retrieving the communication signal and the target response matrix in Problem (4) is both fundamental and challenging. Different from conventional linear LS problem that has a unique solution if the observation matrix has full column rank, solving the equation $\mathbf{A}\mathbf{X} + \mathbf{Z}\mathbf{B} = \mathbf{C}$ naturally provides a non-unique solution set unless other constraints are imposed [21]. In Problem (4), the uniqueness is guaranteed by considering the communication alphabet constraint, which is further investigated in the subsequent sections.

B. SIC-Type Receivers

Previous contributions mainly consider two types of SIC-based schemes to address Problem (4), namely C-SIC and S-SIC [7]. As shown at the top of Fig. 2, C-SIC and S-SIC both use two stages to process the S&C signal where the estimated signal in the first stage is subtracted from the superposed signal in the second stage. In the S-SIC scheme, the receiver first decodes the uplink data by treating the aggregate interference-plus-noise $\mathbf{A}_r\mathbf{h}_r + \mathbf{n}$ as Gaussian noise, and the decoded signal can be obtained by solving the following standard signal detection problem

$$\mathbf{x}_c^{\text{SIC}} = \underset{\mathbf{x}_c \in \mathcal{X}^{LK}}{\text{argmin}} \|\mathbf{y} - \mathbf{A}_c\mathbf{x}_c\|_2^2. \tag{6}$$

Assuming that the uplink data has been perfectly decoded, the detected communication signal is subtracted from the superposed signal. The remainder, $\mathbf{y} - \mathbf{A}_c\mathbf{x}_c^{\text{SIC}}$, is then utilized to estimate the target response matrix $\mathbf{H}_r$ by the standard LS method. When all the communication symbols are successfully detected, the target response estimation can achieve the same performance as the sensing only system. In the C-SIC scheme, the target response vector is first estimated under the communication interference, and the estimated radar signal is subtracted during the communication signal detection. However, the estimation problem can be viewed as a detection problem with infinite hypothesis space, implying that target response estimation errors are inevitable. Thus, the resident target response estimation error influences the subsequent communication performance, indicating that the S&C performance of the C-SIC scheme in two stages is strictly worse than that of the sensing/communication only systems. To fully exploit the potential of uplink ISAC systems, we mainly discuss the S-SIC scheme (which is called the SIC scheme in the rest of the manuscript), while the spirit of the C-SIC scheme is used in designing the block level structure as discussed in Subsection V-B.

The most significant drawback of the SIC scheme in uplink ISAC systems is the ineffective interference processing function. By treating the radar signal as Gaussian noise, the communication signal detection problem in (6) has a low SINR, leading to a high bit error rate (BER) in the first stage. Besides, the residual communication signal detection error becomes more pronounced due to the high BER in the first stage, significantly impacting the target response estimation performance in the second stage, known as error propagation.

C. The Projection-Type Receiver

In our previous work [18], the projection-type receivers were proposed to effectively address the mutual interference. Unlike SIC, our proposed estimation scheme is an equivalent transformation of the ML estimation in (4).

In the following, we present Theorem 1 to decouple the variables in the original mixed integer LS problem and transform it into a signal detection problem.

Theorem 1: The solutions to Problem (4) is equivalent to the combination of the solution for the transformed signal detection Problem (7)

$$\hat{\mathbf{x}}_c = \underset{\mathbf{x}_c \in \mathcal{X}^{LK}}{\text{argmin}} \|\mathbf{\Gamma}(\mathbf{y} - \mathbf{A}_c\mathbf{x}_c)\|_2^2, \tag{7}$$

and the closed-form solution for the target response with the estimated communication symbols $\hat{\mathbf{x}}_c$:

$$\hat{\mathbf{h}}_r(\hat{\mathbf{x}}_c) = \mathbf{\Xi}\mathbf{A}_r^H(\mathbf{y} - \mathbf{A}_c\hat{\mathbf{x}}_c), \tag{8}$$

where $\mathbf{\Xi} = (\mathbf{A}_r^H\mathbf{A}_r)^{-1}$, and $\mathbf{\Gamma} = \mathbf{I}_{LM_r} - \mathbf{A}_r(\mathbf{A}_r^H\mathbf{A}_r)^{-1}\mathbf{A}_r^H$ is the projection matrix of the complement space of $\mathbf{A}_r$.

Proof: Please refer to [18]. ∎

Based on Theorem 1, the projection-based algorithm is provided in [18, Algorithm 1] and at the bottom of Fig. 2. Our proposed projection-type receiver can be regarded as an extension to the SIC scheme with proper interference elimination methodology. Compared to the SIC scheme, we first project the superimposed signal into the complement space of $\mathbf{A}_r$ to eliminate the radar signal interference in the signal detection process. After this projection, we decode the communication signal and subsequently estimate the target response, following a process similar to the SIC method.

It was demonstrated in [18] that the proposed projection-type receivers maintain the same signal-to-noise ratio (SNR) as the communication only systems in the signal detection problem and have lower BER than convention SIC in most cases. Besides, jointly processing multiple snapshots is another key distinction between the projection-type receiver and SIC-type receivers. It was shown that the signal detection performance improves and the communication ergodic achievable rate increases as the number of the snapshots L increases. As $L \to \infty$, the ergodic rate approaches that of the communication only systems, indicating that the impact of the mutual interference can be perfectly canceled.

However, the improved performance comes at the cost of increased complexity. The projection-type receivers require to handle a high-dimensional equivalent channel matrix $\mathbf{G} \triangleq \mathbf{\Gamma}\mathbf{A}_c \in \mathbb{C}^{LM_r \times LK}$ in (7) that scales with the product of the number of transmitted antennas and the number of snapshots. Apart from the largely increased dimension, the performance of the projection-type receiver also suffers from the rank-deficiency issue, i.e., the rank of the equivalent channel matrix $\mathbf{G}$ is smaller than the number of the transmitted symbols. The rank deficiency issue is presented in the following lemma.

Lemma 1: Matrix $\mathbf{G}$ is a singular matrix, and its rank is given by $\text{Rank}(\mathbf{G}) = (L - M_t)K < LK$.

Proof: Please refer to [18]. ∎

Remark 2: From a matrix equation perspective, solving a rank-deficient matrix equation leads to infinity solutions, which is extremely sensitive to the noise. Since the projection-type receivers establish an equivalent transformation of Problem (4), they also maintain the rank deficiency issue, posing a challenge in the communication signal detection problem.

III. FP-TYPE RECEIVERS: A UNIFIED FRAMEWORK

In this section, we first introduce the design principle of the FP-type receivers, which unifies the aforementioned projection-type receivers and the SIC-type receivers with a flexible tradeoff factor. The SINR and the condition number of the formulated signal detection problem using FP-type receivers are then explored. Finally, the PEP of the FP-type receivers using ML detector and linear detector is respectively analyzed.
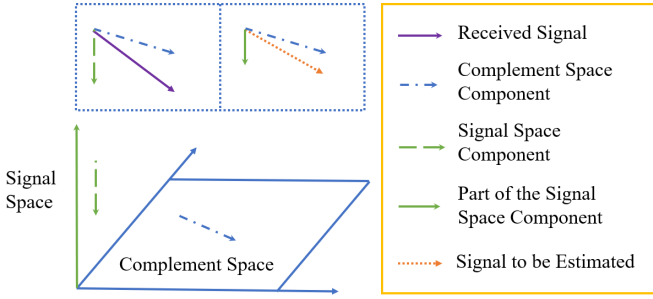
Fig. 3: Illustration of the proposed FP-type receivers

A. Design Principle of the FP-type Receivers

The core of the projection-type receivers is solving the signal detection Problem in (7). In the projection-type receivers, matrix $\mathbf{\Gamma}$ is the orthogonal projection matrix of $\mathbf{A}_r$, which can be rewritten as

$$\mathbf{\Gamma} = \mathbf{P}_\perp \otimes \mathbf{I}_{M_r}, \qquad (9)$$

and the equivalent channel matrix in the signal detection problem (7) is

$$\mathbf{G} = \mathbf{\Gamma}\mathbf{A}_c = \mathbf{P}_\perp \otimes \mathbf{H}_c, \qquad (10)$$

where $\mathbf{P}_\perp = \mathbf{I}_L - \mathbf{X}_r^T(\mathbf{X}_r^*\mathbf{X}_r^T)^{-1}\mathbf{X}_r^*$ is the projection matrix corresponding to the complement space of the radar signal.

It can be observed from (9) and (10) that the formulated signal detection problem in (7) can be modified by changing matrix $\mathbf{P}_\perp$. Besides, the singular values of $\mathbf{G}$ are also determined by those of the orthogonal projection matrix $\mathbf{P}_\perp$, which introduces the rank deficiency issue. Hence, modifying matrix $\mathbf{P}_\perp$ can significantly influence the property of the transformed signal detection problem.

In [18], the received signal is projected to the complement space of the radar signal so that the radar interference is fully eliminated during the signal detection, and is termed as the projection-type receivers. In this work, a more general framework using projection is proposed, termed the FP-type receivers. Defining $\mathbf{P}_\parallel = \mathbf{X}_r^T(\mathbf{X}_r^*\mathbf{X}_r^T)^{-1}\mathbf{X}_r^*$ as the projection matrix corresponding to the signal space of the radar waveform, the projection matrix of FP-type receivers $\mathbf{P}_{\mathrm{FP}}$ is updated according to

$$\mathbf{P}_{\mathrm{FP}} \triangleq (1-\rho)\mathbf{P}_\perp + \rho\mathbf{I}, = \mathbf{P}_\perp + \rho\mathbf{P}_\parallel, \qquad (11)$$

where $\rho \in [0,1]$ is the tradeoff factor. Upon defining $\mathbf{\Gamma}_\parallel = \mathbf{P}_\parallel \otimes \mathbf{I}_{M_r}$ as the projection matrix corresponding to the signal space of $\mathbf{A}_r$, the communication signal detection in the FP-type receivers can be formulated as

$$\hat{\mathbf{x}}_c = \underset{\mathbf{x}_c \in \mathcal{X}^{LK}}{\arg\min} \ \|\mathbf{\Gamma}_{\mathrm{FP}}(\mathbf{y} - \mathbf{A}_c\mathbf{x}_c - \mathbf{A}_r\mathbf{h}_r)\|_2^2 \qquad (12)$$

$$= \underset{\mathbf{x}_c \in \mathcal{X}^{LK}}{\arg\min} \ \| \underbrace{\mathbf{\Gamma}(\mathbf{y} - \mathbf{A}_c\mathbf{x}_c)}_{\substack{\text{Complement Space} \\ \text{Component}}} + \rho\underbrace{\mathbf{\Gamma}_\parallel(\mathbf{y} - \mathbf{A}_c\mathbf{x}_c - \mathbf{A}_r\mathbf{h}_r)}_{\substack{\text{Signal Space} \\ \text{Component}}} \|_2^2.$$

In Fig. 3, we provide an illustration of the proposed FP-type receivers. The received signal is decomposed into the signal space component and the complement space component of matrix $\mathbf{A}_r$. In the proposed FP-type receivers, the communication signal is detected via a reconstructed signal, which is the combination of the complement space component and part of the signal space component. The tradeoff factor ρ

decides the ratio of the signal space component used. More specifically, if the tradeoff factor $\rho = 1$, we have $\mathbf{P}_{\mathrm{FP}} = \mathbf{I}_{M_r}$ and $\mathbf{\Gamma}_{\mathrm{FP}} = \mathbf{I}_{LM_r}$. This means the reconstructed signal is the same as the received signal, which corresponds to the SIC-type receivers. By decreasing the tradeoff factor ρ, the signal space component has less impact on determining the communication symbols. When $\rho = 0$, the received signal is projected to the complement space of the radar signal to fully eliminate the radar interference before the signal detection. In other words, the FP-type receivers are reduced to the projection-type receivers.

Since we do not know any prior information about $\mathbf{h}_r$, a similar methodology as in SIC-type receivers is utilized by treating the signal space component of the radar signal plus noise as the AWGN. Then, Problem (12) can be reformulated as

$$\hat{\mathbf{x}}_c \approx \underset{\mathbf{x}_c \in \mathcal{X}^{LK}}{\arg\min} \ \|\mathbf{\Gamma}_{\mathrm{FP}}(\mathbf{y} - \mathbf{A}_c\mathbf{x}_c)\|_2^2$$

$$= \underset{\mathbf{x}_c \in \mathcal{X}^{LK}}{\arg\min} \ \|\mathbf{y}_{\mathrm{FP}} - \mathbf{G}_{\mathrm{FP}}\mathbf{x}_c\|_2^2, \qquad (13)$$

where

$$\mathbf{y}_{\mathrm{FP}} = (\mathbf{P}_{\mathrm{FP}} \otimes \mathbf{I}_{M_r})\mathbf{y}, \text{ and } \mathbf{G}_{\mathrm{FP}} = \mathbf{P}_{\mathrm{FP}} \otimes \mathbf{H}_c. \qquad (14)$$

After the solution of Problem (13) is obtained, the FP-type receivers then perform the target response estimation with the estimated communication signal $\hat{\mathbf{x}}_c$ according to (8). Since the precision of the target response estimation is largely determined by the performance of the signal detection, the performance of the FP-type receivers is evaluated by the characteristics of Problem (13) in the subsequent analysis.

B. Revealing the Tradeoff Between Condition Number and SINR

In this subsection, we analyze the condition number and the SINR of the transformed signal detection problem using the FP-type receivers.

The condition number of matrix $\mathbf{G}_{\mathrm{FP}}$ characterizes the undesirable correlation between each column of the matrix, which is given by

$$\mathrm{Cond}_{\mathrm{PT}}(\mathbf{G}_T) \triangleq \frac{\omega_1(\mathbf{G}_{\mathrm{FP}})}{\omega_{LNt}(\mathbf{G}_{\mathrm{FP}})} = \sqrt{\frac{\lambda_1(\mathbf{G}_{\mathrm{FP}}^H\mathbf{G}_{\mathrm{FP}})}{\lambda_{LNt}(\mathbf{G}_{\mathrm{FP}}^H\mathbf{G}_{\mathrm{FP}})}}$$

$$= \sqrt{\frac{\lambda_1(\mathbf{P}_{\mathrm{FP}}^H\mathbf{P}_{\mathrm{FP}})\lambda_1(\mathbf{H}_c^H\mathbf{H}_c)}{\lambda_L(\mathbf{P}_{\mathrm{FP}}^H\mathbf{P}_{\mathrm{FP}})\lambda_{Nt}(\mathbf{H}_c^H\mathbf{H}_c)}} \qquad (15)$$

$$= \frac{\lambda_1(\mathbf{P}_{\mathrm{FP}})}{\lambda_L(\mathbf{P}_{\mathrm{FP}})}\mathrm{Cond}(\mathbf{H}_c) \overset{(a)}{=} \frac{1}{\rho}\mathrm{Cond}(\mathbf{H}_c),$$

where (a) exploits the fact that $\mathbf{P}_\perp$ has $L-M_t$ unit eigenvalues as well as M_t zero eigenvalues, and for arbitrary matrix $\mathbf{A} \in \mathbb{C}^{N \times N}$, $\lambda_i(\mathbf{A} + \sigma\mathbf{I}) = \lambda_i(\mathbf{A}) + \sigma, i = 1, \cdots, N$.

This indicates that with a smaller tradeoff factor, the column correlation increases, leading to an ill-conditioned equivalent channel matrix and worse signal detection performance.

Lemma 2: The SINR of the transformed signal detection problem using the FP-type receivers is given by

$$\mathrm{SINR}_{\mathrm{FP}} \triangleq \frac{\mathbb{E}\left[\|\mathbf{\Gamma}_{\mathrm{FP}}\mathbf{A}_c\mathbf{x}_c\|_2^2\right]}{\mathbb{E}\left[\|\mathbf{\Gamma}_{\mathrm{FP}}\mathbf{A}_r\mathbf{h}_r\|_2^2\right] + \mathbb{E}\left[\|\mathbf{\Gamma}_{\mathrm{FP}}\mathbf{n}\|_2^2\right]}$$

$$= \frac{P_c(L - (1-\rho^2)M_t)KM_r}{\rho^2 LP_s + (L - (1-\rho^2)M_t)M_rK\sigma^2}, \qquad (16)$$

which is a monotonic decreasing function of the tradeoff factors ρ. The maximum and the minimum SINR are, respectively, achieved by using the projection-type and the SIC-type receivers.

Proof: Please refer to Appendix A. ∎

Remark 3: From the geometry perspective, the received signal that lies in the complement space has a higher SINR as compared to the signal space component. However, directly projecting the received signal to the complement space reduces the dimension of the observation signal, leading to a correlated equivalent channel matrix. By increasing the tradeoff factor ρ, the channel correlation is decreased owing to the introduced signal space component, which, however, also leads to a decreased SINR.

C. PEP Analysis of the FP-type Receivers

The condition number and SINR of the signal detection problem derived in the last subsection characterize the property of the formulated problem from different aspects. The error probability P_e under different algorithms is a more direct performance metric, which however is generally computationally intractable. A customary solution is to approximate the error probability using the PEP. The PEP is defined as the probability that $\bar{\mathbf{x}}_c$ is selected at the receivers when $\tilde{\mathbf{x}}_c$ is transmitted, i.e., $P(\tilde{\mathbf{x}}_c \to \bar{\mathbf{x}}_c)$. The connection between the error probability and PEP can be characterized by

$$P_e \leq \frac{1}{|\mathcal{X}|} \sum_{\tilde{\mathbf{x}}_c \in \mathcal{X}} \sum_{\bar{\mathbf{x}}_c \in \mathcal{X} \backslash \tilde{\mathbf{x}}_c} P(\tilde{\mathbf{x}}_c \to \bar{\mathbf{x}}_c). \tag{17}$$

In what follows, we analyze the PEP of the FP-type receivers when using the ML detector and ZF detector, respectively.

ML detector uses an exhaustive searching method to find the solution to Problem (13) and typically serves as the performance upper bound of the signal detection algorithm. Denoting $\boldsymbol{\delta} = \tilde{\mathbf{x}}_c - \bar{\mathbf{x}}_c$, the PEP under the ML criterion is given by [22, Chapter 15]

$$\begin{aligned} P_{\mathrm{ML}}(\tilde{\mathbf{x}}_c \to \bar{\mathbf{x}}_c) &= P\left(\|\tilde{\mathbf{y}} - \mathbf{G}_{\mathrm{FP}}\tilde{\mathbf{x}}_c\|_2 \leq \|\tilde{\mathbf{y}} - \mathbf{G}_{\mathrm{FP}}\bar{\mathbf{x}}_c\|_2\right) \\ &= Q\left(\frac{\|\mathbf{G}_{\mathrm{FP}}\boldsymbol{\delta}\|_2}{\sqrt{2\sigma_{\mathrm{ML}}^2}}\right), \end{aligned} \tag{18}$$

where Q denotes the Q-function and

$$\begin{aligned} \sigma_{\mathrm{ML}}^2 &= \rho^2 \mathbb{E}\left[\|\mathbf{A}_r \mathbf{h}_r\|_2^2\right] + \mathbb{E}\left[\|\boldsymbol{\Gamma}_{\mathrm{FP}}\mathbf{n}\|_2^2\right] \\ &= \rho^2 L P_s + (L - (1-\rho^2)M_t)K M_r \sigma^2. \end{aligned} \tag{19}$$

Defining $\boldsymbol{\Delta} = \mathrm{Unvec}(\boldsymbol{\delta})$ and using the equation $\mathrm{vec}(\mathbf{ABC}) = (\mathbf{C}^{\mathrm{T}} \otimes \mathbf{A})\,\mathrm{vec}(\mathbf{B})$, (18) can be rewritten as

$$P_{\mathrm{ML}}(\tilde{\mathbf{x}}_c \to \bar{\mathbf{x}}_c) = Q\left(\frac{\|\mathbf{H}_c \boldsymbol{\Delta} \mathbf{P}_{\mathrm{FP}}^*\|_F}{\sqrt{2\sigma_{\mathrm{ML}}^2}}\right). \tag{20}$$

To derive the analytical results and provide guidance to the FP-type receiver design, the following two assumptions are made.

Assumption 1: Assuming that the number of received antennas at the BS goes infinity, i.e., $M_r \to \infty$, and each entry of the channel matrix follows the complex Gaussian distribution, we have $\mathbf{H}_c^{\mathrm{H}}\mathbf{H}_c \approx \mathbf{I}$. This assumption is known as the favorable propagation in large-scale MIMO systems

and is widely used in reducing the complexity of the MIMO precoding and signal detection [23]. The favorable propagation assumption may not necessarily hold true in practical systems. However, adopting this assumption provides a theoretical upper bound of the PEP for ML detection and helps derive the analytical results.

Assumption 2: The transmission process is defined as transmitting L snapshots at a time block by K CUs. We assume that during each transmission, only one transmitted symbol is incorrectly detected. This assumption holds true if the SINR is not very small given that the number of the snapshots is not very large. Without loss of generality, we assume that only the transmitted symbol at the N_1-th antenna in the L_1-th snapshot is incorrectly detected, then (p,q)-th elements of $\boldsymbol{\Delta}$ follows

$$\boldsymbol{\Delta}_{[p,q]} = \begin{cases} d_{\min}, & p, q = N_1, L_1 \\ 0, & \text{else}, \end{cases} \tag{21}$$

where $d_{\min}$ is the minimum distance in the constellation.

By using the above 2 assumptions, the expectation of $P_{\mathrm{ML}}(\tilde{\mathbf{x}}_c \to \bar{\mathbf{x}}_c)$ over $\boldsymbol{\Delta}$ can be approximated as

$$\begin{aligned} \mathbb{E}\left[P_{\mathrm{ML}}(\tilde{\mathbf{x}}_c \to \bar{\mathbf{x}}_c)\right] &\approx Q\left(\frac{d_{\min}\|\mathbf{P}_{\mathrm{FP}}^*\|_F}{L\sqrt{2\sigma_{\mathrm{ML}}^2}}\right) \\ &= Q\left(\frac{d_{\min}\sqrt{L - (1-\rho^2)M_t}}{L\sqrt{2\sigma_{\mathrm{ML}}^2}}\right). \end{aligned} \tag{22}$$

It can be easily verified that for the FP-type receivers, the approximate PEP is an increasing function of ρ, indicating that the projection-type receivers are optimal if ML detection is used.

The performance of the linear estimator usually serves as the lower bound of the system performance. When $\rho \in (0,1]$, the PEP based on the ZF detector is given by [24]

$$P_{\mathrm{ZF}}(\mathbf{x} \to \bar{\mathbf{x}}) = Q\left(\frac{\|\boldsymbol{\Delta}\|_F^2}{\sqrt{2\sigma_{\mathrm{ZF}}^2}}\right), \tag{23}$$

where

$$\sigma_{\mathrm{ZF}}^2 = \sigma_{\mathrm{ML}}^2 \|\mathbf{G}_{\mathrm{FP}}^\dagger \boldsymbol{\delta}\|_2^2 = \sigma_{\mathrm{ML}}^2 \|\mathbf{H}_c^\dagger \boldsymbol{\Delta}(\mathbf{P}_{\mathrm{FP}}^\dagger)^*\|_F^2. \tag{24}$$

By adopting Assumption 1, σ_{ZF}^2 can be approximated as follows

$$\sigma_{\mathrm{ZF}}^2 \approx \sigma_{\mathrm{ML}}^2 \|\mathbf{H}_c \boldsymbol{\Delta}(\mathbf{P}_{\mathrm{FP}}^\dagger)^*\|_F^2 \approx \sigma_{\mathrm{ML}}^2 \|\boldsymbol{\Delta}(\mathbf{P}_{\mathrm{FP}}^\dagger)^*\|_F^2. \tag{25}$$

By adopting Assumption 2, the expectation of $P_{\mathrm{ZF}}(\tilde{\mathbf{x}}_c \to \bar{\mathbf{x}}_c)$ over $\boldsymbol{\Delta}$ can be further approximated by

$$\begin{aligned} \mathbb{E}\left[P_{\mathrm{ZF}}(\tilde{\mathbf{x}}_c \to \bar{\mathbf{x}}_c)\right] &= Q\left(\frac{d_{\min}^2}{\sqrt{2\sigma_{\mathrm{ZF}}^2}}\right) \\ &\approx Q\left(\frac{d_{\min}^2 L}{d_{\min}\sqrt{2\sigma_{\mathrm{ML}}^2\|\mathbf{P}_{\mathrm{FP}}^\dagger\|_F^2}}\right) \\ &= Q\left(\frac{d_{\min}L}{\sqrt{2\sigma_{\mathrm{ML}}^2(L - M_t + \frac{M_t}{\rho^2})}}\right). \end{aligned} \tag{26}$$

This means that the equivalent noise of the ZF detector σ_{ZF}^2 is determined not only by the equivalent noise of the ML

detector σ_{ML}^2, but also by the "noise amplification" effect of the pseudo-inverse of matrix $\mathbf{P}_{\mathrm{FP}}$. When $\rho \rightarrow 0$, the matrix $\mathbf{P}_{\mathrm{FP}}$ is reduced to the projection-type receivers, which theoretically have infinity noise. Therefore, conventional projection-type receivers are not suitable for the ZF detector.

Remark 4: From the previous analysis, we find that the projection-type receivers have better performance if a "strong" signal detector is applied, while the conventional SIC method is more suitable if a simple MIMO signal detection estimator is used. In other words, the projection-type receivers have a higher performance upper bound, while the SIC-type receivers have a higher performance lower bound when the detection algorithm is relatively simple.

Remark 5: By setting the first order partial derivation of $\frac{\partial(26)}{\partial \rho}$ to zero, the optimal tradeoff factor is a function of P_{r} and σ^2. This indicates that, when a specific MIMO signal detection algorithm is applied, the optimal tradeoff factor that achieves the best signal detection performance is related to the S&C power and noise density. In other words, the optimal tradeoff factor should be environment adaptive, and we can not expect one FP-type receivers such as projection-type receivers or SIC-type receivers to achieve the desired performance in various scenarios.

IV. LOW COMPLEXITY ALGORITHM DEVELOPMENT

Deriving a suitable algorithm for solving the transformed signal detection problem in (13) is quite challenging due to its large dimension and ill-conditioned issues. Specifically, most low complexity algorithms, such as message passing [25], [26], approximate matrix inverse [27], do not exploit the alphabet constraint in algorithm development, yielding poor performance when the equivalent channel matrix is ill-conditioned, or even rank-deficient. On the other hand, many performance-guaranteed algorithms in rank-deficient environments such as sphere decoding [28] and the semi-definite relaxation (SDR) method [29], often entail high computational complexity considering the high dimensionality of $\mathbf{G}$.

In this section, we first introduce the homotopy optimization framework, which is then utilized to solve the signal detection problem in (13). Finally, a tailed low-complexity solution, namely, DFP-type receivers, is presented. As compared to the FP-type receivers, the DFP-type receivers can achieve better path-tracing performance and enhanced environmental adaptability.

A. Homotopy Optimization Framework

In general, the homotopy optimization method is a type of path-tracing algorithm that is designed to solve complex, nonlinear, and often non-convex optimization problems. The central idea of homotopy optimization is to transform the original difficult optimization problem into a set of simpler problems by introducing a continuous transformation parameter. This parameter gradually deforms the objective function from a simple starting function to the target function that represents the original problem [30].

The key to homotopy optimization is to find a proper surrogate function called the homotopy function. Assuming that we are interested in finding the optimal solution of the following problem via homotopy optimization method

$$\mathbf{z}^* = \arg\min f(\mathbf{z}). \tag{27}$$

We need to find a continuous homotopy function $h(\mathbf{z}, \eta)$ so that

$$h(\mathbf{z}, \eta) = \begin{cases} f^0(\mathbf{z}), & \text{if } \eta = 0 \text{ and} \\ f^1(\mathbf{z}), & \text{if } \eta = 1, \end{cases}$$

where $f^0(\mathbf{z}) = f(\mathbf{z})$ and finding the minimizer of $f^1(\mathbf{z})$ is much easier as compared to $f^0(\mathbf{z})$.

The homotopy optimization starts with solving the minimization problem with $f^1(\mathbf{z})$ as the objective function. By gradually adjusting η from 1 to 0, the problem evolves, and the solution of the previous minimization problem serves as an initial point of the newly formulated problem. This allows the optimizer to trace the path of the solution, and as the transformation progresses, the minimizer converges to the minimizer of the original, more challenging problem. Overall, the implementation details of the homotopy optimization method are summarized in Algorithm 1.

Algorithm 1 Homotopy optimization Framework

Input: initial point $\mathbf{z}^0$, a decreasing sequence $\eta^l, l = 1, \cdots, L$ that satisfies $\eta^1 = 1$, $\eta^{l_{\max}} = 0$.
Output: The optimized result $\tilde{\mathbf{z}} = \mathbf{z}^{l_{\max}}$.

1: $l = 1$
2: **Repeat**
3: Use a local minimization method, starting with $\mathbf{z}^{(l-1)}$, to compute an (approximate) solution $\mathbf{z}^{(l)}$ to $\arg\min h(\mathbf{z}, \eta^l)$.
4: $l = l + 1$.
5: **Until** $l = l_{\max}$

B. Homotopy-based MIMO Signal Detection Algorithm

In this subsection, we introduce a homotopy-based MIMO signal detection algorithm presented in [31], [32]. The authors of [31], [32] first found the homotopy function by proposing an equivalent transformation of the MIMO signal detection problem. Subsequently, a projected gradient (PG) method is used under the homotopy optimization framework. In the following, we introduce how to utilize this MIMO signal detection algorithm to solve Problem (13) in the FP-type receivers, which also serves as the basis of our subsequent design.

By letting

$$\overline{\mathbf{y}} = \begin{bmatrix} \mathrm{Re}(\mathbf{y}_{\mathrm{FP}}) \\ \mathrm{Im}(\mathbf{y}_{\mathrm{FP}}) \end{bmatrix}, \quad \overline{\mathbf{x}} = \begin{bmatrix} \mathrm{Re}(\mathbf{x}_{\mathrm{c}}) \\ \mathrm{Im}(\mathbf{x}_{\mathrm{c}}) \end{bmatrix}, \tag{28}$$

and

$$\overline{\mathbf{G}} = \begin{bmatrix} \mathrm{Re}(\mathbf{G}_{\mathrm{FP}}) & -\mathrm{Im}(\mathbf{G}_{\mathrm{FP}}) \\ \mathrm{Im}(\mathbf{G}_{\mathrm{FP}}) & \mathrm{Re}(\mathbf{G}_{\mathrm{FP}}) \end{bmatrix}, \tag{29}$$

Problem (13) can be rewritten as

$$\min_{\overline{\mathbf{x}} \in \mathcal{X}_{\mathrm{R}}^{2LK}} f(\overline{\mathbf{x}}) = \|\overline{\mathbf{y}} - \overline{\mathbf{G}}\overline{\mathbf{x}}\|_2^2, \tag{30}$$

where $\overline{\mathbf{x}} \in \mathcal{X}_{\mathrm{R}}^{2LK}$ denotes the real-valued alphabet constraint.

The main challenge of solving Problem (30) lies in the discrete alphabet constraint. In the following theorem, we show that the homotopy function can be constructed by relaxing the alphabet constraint into its convex hull and penalization.

Theorem 2: Problem (31) is an equivalent transformation of Problem (30) if the penalty parameter $\mu > \lambda_1(\overline{\mathbf{G}}^{\mathrm{T}}\overline{\mathbf{G}})$,

$$\min_{\overline{\mathbf{x}} \in \mathrm{conv}(\mathcal{X}_{\mathrm{R}})} F_\mu(\overline{\mathbf{x}}) = f(\overline{\mathbf{x}}) - \mu\|\overline{\mathbf{x}}\|_2^2$$
$$= \overline{\mathbf{x}}^{\mathrm{T}}\left(\overline{\mathbf{G}}^{\mathrm{T}}\overline{\mathbf{G}} - \mu\mathbf{I}\right)\overline{\mathbf{x}} - 2\overline{\mathbf{y}}^{\mathrm{T}}\overline{\mathbf{G}}^{\mathrm{T}}\overline{\mathbf{x}} + \|\overline{\mathbf{y}}\|_2^2. \quad (31)$$

Proof: $F_\mu(\overline{\mathbf{x}})$ is strictly concave since $\overline{\mathbf{G}}^{\mathrm{T}}\overline{\mathbf{G}} - \mu\mathbf{I}$ is negative definite. Theorem 2 can be proved by using the conclusion in [33, Section 32]. ∎

While Problem (31) is still a highly non-convex and hard to solve problem due to its non-concave objective function, the homotopy optimization method can be adopted with a gradually increasing penalty sequence $\mu_l, l = 1, \cdots, l_{\max}$. Intuitively, when the penalty parameter μ is small: on the one hand, the gap between Problem (30) and Problem (31) is large, which potentially means that constraint $\overline{\mathbf{x}} \in \mathcal{X}_{\mathrm{R}}$ may not be satisfied; On the other hand, the convexity of Problem (31) is better preserved, suggesting that it is easier to obtain the optimal solution of Problem (31). Considering these properties, we start with a small value of μ (i.e., $\mu_1 = 0$) and solve Problem (31) with gradually increasing μ_l in l-th iteration. Finally, with a sufficiently large value of μ_l, we can gradually approach the optimal solution to Problem (13).

With a fixed value of μ_l, Problem (31) can be solved using the PG method [34]. The PG method is a low-complexity iterative algorithm that alternates between gradient descent and projection. In conventional MIMO signal detection problems, such as Problem (30), projection involves rounding to the discrete constellation, leading to conflicting effects as the performance of the PG method approaches that of the linear decoder [35]. Specifically, during the gradient descent stage, the solutions move toward the non-constrained LS problem, while the subsequent projection to the discrete constellation diminishes the effectiveness of the earlier process.

When the original MIMO signal detection problem is rewritten into the continuous function in (31), the gradient descent step and the projection step of the PG algorithm have been modified. First, gradient descent is applied at the majorant of $F_\mu(\overline{\mathbf{x}})$. The majorant of $F_\mu(\overline{\mathbf{x}})$ at the k-th step $\overline{\mathbf{x}}^k$ is obtained by replacing $\|\overline{\mathbf{x}}\|_2^2$ with its first-order approximation, given by

$$G_\mu(\overline{\mathbf{x}} \mid \overline{\mathbf{x}}^k) = f(\overline{\mathbf{x}}) - 2\mu_l\langle\overline{\mathbf{x}}^k, \overline{\mathbf{x}} - \overline{\mathbf{x}}^k\rangle - \mu_l\|\overline{\mathbf{x}}^k\|^2. \quad (32)$$

Thus, the gradient of $G_\mu(\overline{\mathbf{x}} \mid \overline{\mathbf{x}}^k)$ is given by

$$\nabla_{\overline{\mathbf{x}}} G_\mu\left(\overline{\mathbf{x}} \mid \overline{\mathbf{x}}^k\right) = 2\overline{\mathbf{G}}^{\mathrm{T}}\overline{\mathbf{G}}\overline{\mathbf{x}} - 2\overline{\mathbf{G}}^{\mathrm{T}}\overline{\mathbf{y}} - 2\mu_l\overline{\mathbf{x}}^k. \quad (33)$$

Second, the projection operation is performed on the continuous convex hull of the original alphabet constraints $\mathrm{conv}(\mathcal{X}_{\mathrm{R}})$. Given that the alphabet constraints in most modulation schemes, such as phase shift keying (PSK) and quadrature amplitude modulation (QAM), can be written as constant modulus constraints [32]. The projection to these constant modulus constraints is usually computationally effective and

also better at utilizing gradient information, thereby accelerating convergence speed.

Here we take 4-QAM as an example to show the benefit of applying the transformation in Theorem 2. When the PG method is directly applied at Problem (30), the projection is performed at the constellation constraint $\overline{\mathbf{x}} \in \{-1, 1\}^n$, which means deciding each transmitted symbol according to its signature. In contrast, with homotopy optimization, the projection is performed at the convex hull of the constellation constraint, $\mathrm{conv}\left(\{-1, 1\}^n\right) = [-1, 1]^n$. As a result, the projection operation becomes $\Pi_{\mathcal{X}}(\mathbf{x}) = \left[\Pi\left(x_1\right), \ldots, \Pi\left(x_N\right)\right]^{\mathrm{T}}$, where

$$\Pi(x) = \begin{cases} -1, & x < -1 \\ x, & -1 \le x \le 1. \\ 1, & x > 1 \end{cases} \quad (34)$$

Thus, the projection in (34) tends to become smoother for $-1 \le x \le 1$, making the PG method much easier to get rid of the local optimal solution.

C. DFP-type Receiver Designs

While the aforementioned algorithm can efficiently address the transformed MIMO signal detection problem, it still faces the dilemma of selecting the proper value of ρ. Besides, the FP-type receiver fails to establish the equivalence between Problem (13) and Problem (4). In this regard, we propose to further apply the spirits of the homotopy optimization, which further leads to DFP-type receivers. In Lemma 3, we provide a theoretical foundation for the proposed DFP-type receivers.

Lemma 3: Problem (35) is an equivalent transformation of Problem (4) if $\mu > \lambda_1(\mathbf{H}_{\mathrm{c}}^{\mathrm{H}}\mathbf{H}_{\mathrm{c}})$, and $\rho = 0$,

$$\min_{\overline{\mathbf{x}} \in \mathrm{conv}(\mathcal{X}_{\mathrm{R}})} F_{\mu,\rho}(\overline{\mathbf{x}}) = \overline{\mathbf{x}}^{\mathrm{T}}\left(\overline{\mathbf{G}}^{\mathrm{T}}(\rho)\overline{\mathbf{G}}(\rho) - \mu\mathbf{I}\right)\overline{\mathbf{x}}$$
$$- 2\overline{\mathbf{y}}^{\mathrm{T}}(\rho)\overline{\mathbf{G}}^{\mathrm{T}}(\rho)\overline{\mathbf{x}} + \|\overline{\mathbf{y}}\|_2^2, \quad (35)$$

where $\overline{\mathbf{G}}(\rho)$ and $\overline{\mathbf{y}}(\rho)$ are a function of ρ as defined in equation (28) and (29).

Proof: Please refer to Appendix B. ∎

Remark 5: Different from the conventional homotopy optimization framework, which introduces an auxiliary variable to transform complex problems into more solvable ones. Two auxiliary variables are introduced to establish the equivalence between the newly formulated Problem (35) and the original problem in (4). Therefore, more DoFs in algorithm development are provided. In the following, we introduce the structure and implementation details of the DFP-type receivers.

As shown in Fig. 4, the communication signal detection process in the DFP-type receivers can be interpreted as a two-loop iterative algorithm which can be divided into three parts.

In the l-th outer iteration, both the penalty parameter μ_l and the tradeoff factor ρ_l update, as shown in the first part of Fig. 4. The first part is the major difference between the DFP-type receivers and the FP-type receivers. Particularly, the tradeoff factor ρ updates in each outer layer iteration according to the predefined sequence $\rho_l, l = 0, \cdots, l_{\max}$, and ρ_l at the l-th iteration is heuristically chosen as

$$\rho_l = \epsilon^l, \epsilon < 1. \quad (36)$$

This exponentiation expression ensures that $\rho_0 = 1$ and with an adequate number of iterations, $\rho_l \to 0$. Then, in each iteration, the matrix $\mathbf{P}_l = \mathbf{P}(\rho_l)$, the vector $\mathbf{y}_l = \overline{\mathbf{y}}(\rho_l)$ and the matrix $\mathbf{G}_l = \overline{\mathbf{G}}(\rho_l)$ are, respectively, updated according to equation (11) and (14).

In the inner layer, the PG algorithm is applied, as shown in the second and the third part of Fig. 4. The second part includes a modification of the conventional gradient descent algorithm, called gradient extrapolated majorization-minimization [36]. More specifically, the gradient descent at the k-th step is performed on the linear combination of the current point $\overline{\mathbf{x}}^k$ and previous point $\overline{\mathbf{x}}^{k-1}$, which is called the extrapolated point $\mathbf{z}^k$ as follows

$$\mathbf{z}^k = \alpha_k(\overline{\mathbf{x}}^k - \overline{\mathbf{x}}^{k-1}) + \overline{\mathbf{x}}^k. \tag{37}$$

Here, the linear combination coefficients sequence α_k is chosen from a predefined sequence as the design in [31].

The third part is to perform the gradient descent function on the extrapolated point $\mathbf{z}^k$. The step size of the gradient descent β^k is chosen as $\beta^k = 1/\|\mathbf{G}_l\|_2$ to fulfill the sufficient descent condition of the quadratic function. Then, the point after gradient descent $\mathbf{t}^k$ is given by

$$\begin{aligned} \mathbf{t}^k &= \mathbf{z}^k - \beta^k \nabla_{\overline{\mathbf{x}}} G_\mu \left(\mathbf{z}^k \mid \overline{\mathbf{x}}^k \right) \\ &= \mathbf{z}^k - 2\beta^k \mathbf{G}_l^{\mathrm{T}} \mathbf{G}_l \mathbf{z}^k + 2\beta^k \mathbf{G}_l^{\mathrm{T}} \mathbf{y}_l + 2\beta^k \mu_l \overline{\mathbf{x}}^k. \end{aligned} \tag{38}$$

Finally, the estimated transmit signal at $k + 1$-th iteration can be obtained by projecting $\mathbf{t}^k$ onto the convex hull of the real-valued alphabet constraint $\mathrm{conv}(\mathcal{X}_{\mathrm{R}})$,

$$\overline{\mathbf{x}}^{k+1} = \Pi\left(\mathbf{t}^k\right). \tag{39}$$

The overall algorithm of the DFP-type receiver designs is summarized in Algorithm 2, whose performance is affected by the choice of the initial point. Therefore, it is crucial to select an initial point that not only enhances algorithm performance, but also maintains low computational complexity. In the DFP-type receivers, we start with the ZF decoder. By exploiting the Kronecker structure, the inverse in ZF detector can be computed efficiently: $\mathbf{G}_{\mathrm{FP}}^\dagger = \mathbf{P}_{\mathrm{FP}}^\dagger \otimes \mathbf{H}_{\mathrm{c}}^\dagger$. Since $\mathbf{P}_{\mathrm{FP}}^\dagger$ can be computed offline, the computational complexity is roughly given by $\mathcal{O}\left(K^3\right)$, irrelevant to the length of the snapshots. Given that only the matrix multiplication is involved in the gradient descent and projection operations, the overall computational complexity of the communication signal detection is roughly given by $\mathcal{O}\left(L^2 K^2\right) + \mathcal{O}\left(K^3\right)$, and the computational complexity corresponding to the target response estimation is given by $\mathcal{O}\left(L^3 M_t^3\right)$, same as the sensing only systems.

In summary, adopting the DFP-type receivers instead of the fixed tradeoff factor FP-type receivers has two benefits. Firstly, the proposed algorithm has a more smooth path-tracing ability to the original problem, thereby reducing the hardness of solving Problem (4). Secondly, although we can not obtain the "optimal and environment adaptive" tradeoff factor as discussed in Remark 5, we are using a "heuristic searching method" with an increased diversity than the fixed tradeoff factor FP-type receivers. Hence, the DFP-type receivers are expected to be more robust in various scenarios.

Algorithm 2 Proposed algorithm for DFP-type receiver designs

1: **Input**: The maximum outer layer iteration time $l_{\max}$, the maximum inner layer iteration time $k_{\max}$, the penalty sequence $\{\mu_l\}$, the step size sequence $\{\beta^k\}$ and a starting point $\overline{\mathbf{x}}_0$.
2: **Output**: Estimated communication signal $\hat{\mathbf{x}}_{\mathrm{c}}$, and estimated target response matrix $\hat{\mathbf{h}}_{\mathrm{r}}$.
3: $l \leftarrow 0$
4: **repeat**
5:     Update $\mathbf{G}_l$ and $\mathbf{y}_l$ according to equation (11) and (14),
6:     Set $k \leftarrow 0$, $\overline{\mathbf{x}}^0 \leftarrow \overline{\mathbf{x}}_l$,
7:     **repeat**
8:        Update the extrapolated point $\mathbf{z}^k$ according to (37).
9:        Obtain $\mathbf{t}^k$ by using the gradient descent in equation (38).
10:       Obtain $\overline{\mathbf{x}}^{k+1}$ by projecting $\mathbf{t}^k$ using equation (39).
11:       $k \leftarrow k + 1$.
12:     **until** $k = k_{\max}$.
13:     $\overline{\mathbf{x}}_{l+1} \leftarrow \overline{\mathbf{x}}^k$
14:     $l \leftarrow l + 1$
15: **until** $l = l_{\max}$.
16: $\hat{\mathbf{x}}_{\mathrm{c}} = \overline{\mathbf{x}}_l$.
17: Estimate the target response vector $\hat{\mathbf{h}}_{\mathrm{r}}$ with the decoded signal $\hat{\mathbf{x}}_{\mathrm{c}}$ according to (8).

V. EXTENSION

A. PDFP-type receiver designs

The adoption of DFP-type receivers has significantly enhanced the environment adaptation compared to FP-type receivers. However, their adaptive ability is still limited by the selection of the predefined tradeoff sequence $\rho_l = \epsilon^l$. For instance, when ϵ is small, the receivers quickly converge to projection-type receivers, making them more suitable when the sensing signal power is strong, but less effective when the sensing signal power is weak. To further improve environment adaptation, parallel DFP (PDFP)-type receivers can be used, consisting of multiple DFP-type receivers. In PDFP-type receivers, we assume that P DFP-type receivers simultaneously perform the communication signal detection using different convergence speeds. The decreasing sequence of the tradeoff factor for p-th receiver is chosen as $\rho_{l,p} = \epsilon_p^l, p = 1, \cdots, P$. Once the estimated communication signal $\hat{\mathbf{x}}_{\mathrm{c},p}$, and the target response vector $\hat{\mathbf{h}}_{\mathrm{r},p}$ of all P receivers is obtained, the final communication signal and target response matrix are chosen based on the detector with the minimum square error:

$$\hat{\mathbf{x}}_{\mathrm{c}}, \hat{\mathbf{h}}_{\mathrm{r}} = \underset{\hat{\mathbf{x}}_{\mathrm{c},p}, \hat{\mathbf{h}}_{\mathrm{r},p}, p \in \{1, \ldots, P\}}{\arg\min} \left\| \mathbf{y} - \mathbf{A}_{\mathrm{c}} \hat{\mathbf{x}}_{\mathrm{c},p} - \mathbf{A}_{\mathrm{r}} \hat{\mathbf{h}}_{\mathrm{r},p} \right\|_2^2. \tag{40}$$

B. Employing Block Structure to Enhance Uplink ISAC Receivers

The previous design primarily focused on developing an algorithm to solve Problem (4), but two additional implementation issues must be addressed. The first question is how many snapshots should be processed jointly. This choice not only
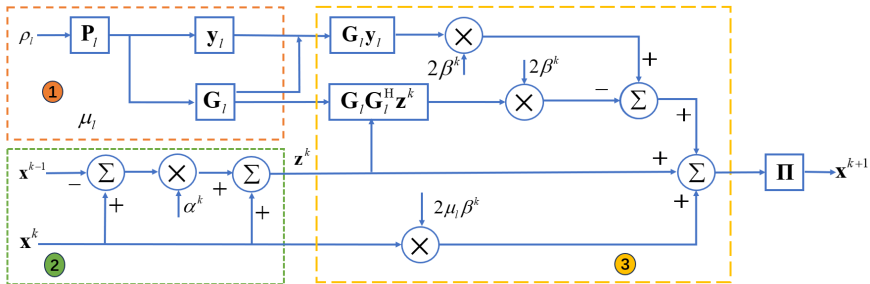
Fig. 4: Illustration of the proposed DFP-type receiver designs

Fig. 5: Block structure of the receiver designs in uplink ISAC systems

impacts the computational complexity but also significantly affects the S&C performance. For communication signal detection, increasing the number of snapshots helps alleviate the rank deficiency issue. Specifically, with the constellation constraint, solving Problem (4) (or equivalently Problem (7)) reduces to finding the intersection of the solution space of the equation $\mathbf{\Gamma y} = \mathbf{G x}_c$ (with dimension $M_t K$) and the constellation constraint $\mathbf{x}_c \in \mathcal{X}^{LK}$. By increasing the number of snapshots L, this intersection narrows, resulting in a lower BER. A heuristic choice for L that typically achieves the desired performance is $L \approx M_t + K$. On the other hand, radar techniques such as multi-pulse accumulation require a large number of snapshots (i.e., $L \gg M_t$) to improve sensing performance. However, processing such a large number of snapshots significantly increases the computational complexity of communication signal detection. The second question is how prior information of the target response matrix, if available, can be utilized to further enhance the performance of the proposed algorithm.

To address the above two problems, a block structure is proposed that ensures fixed algorithmic complexity while exploiting the prior information of the target. As shown in Fig. 5, the overall snapshots are divided into I blocks, which are constituted by J sub blocks. The length of the sub block is determined by the communication setup, for instance, $L \approx M_t + K$, and the number of the sub block or equivalently the length of the block is determined by the sensing requirement. The communication signal detection is performed in each sub block with the aid of the estimation results of the target response matrix from the previous block. Then, the performance gap between Problem (12) and Problem (13) can be decreased given the estimated target response matrix. Specifically, the estimation results of the target response matrix from the previous block $\mathbf{h}_{r,i-1}$ are used to approximate the exact value of $\mathbf{h}_r$. Thus, Problem (12) can be reformulated as

$$
\begin{aligned}
\hat{\mathbf{x}}_c &= \underset{\mathbf{x}_c \in \mathcal{X}^{LK}}{\arg\min} \|\mathbf{\Gamma}(\mathbf{y} - \mathbf{A}_c \mathbf{x}_c) + \rho \mathbf{\Gamma}_\|(\mathbf{y} - \mathbf{A}_c \mathbf{x}_c - \mathbf{A}_r \mathbf{h}_r)\|_2^2 \\
&= \underset{\mathbf{x}_c \in \mathcal{X}^{LK}}{\arg\min} \|\mathbf{\Gamma}_{\mathrm{FP}}(\mathbf{y} - \mathbf{A}_r \mathbf{h}_{r,i-1} - \mathbf{A}_c \mathbf{x}_c) \\
&\qquad + \rho \mathbf{\Gamma}_\| \mathbf{A}_r (\mathbf{h}_r - \mathbf{h}_{r,i-1})\|_2^2 \qquad\qquad (41) \\
&\approx \underset{\mathbf{x}_c \in \mathcal{X}^{LK}}{\arg\min} \|\mathbf{\Gamma}_{\mathrm{FP}}(\mathbf{y} - \mathbf{A}_r \mathbf{h}_{r,i-1} - \mathbf{A}_c \mathbf{x}_c)\|_2^2.
\end{aligned}
$$

From the above derivation, the signal space component of the target response estimation error instead of that of the target
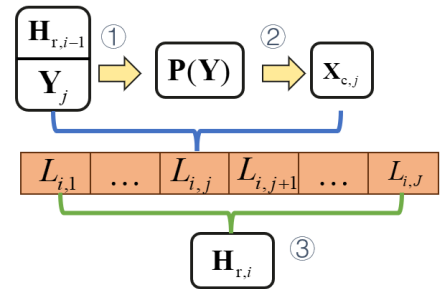
response vector, is treated as the AWGN, greatly improving the SINR. This is essentially similar to the spirits of the C-SIC type receivers, where the sensing signal is first subtracted from the received signal before applying a general projection-type receiver.

After the communication signal of all the J sub blocks is obtained, the target response vector can be estimated by combining the overall J sub blocks. Thus, using the block structure to improve the receivers' performance can be interpreted as a combination of the S-SIC scheme and the C-SIC scheme, where the target response estimation is performed in the long term and the communication signal detection is performed in the short term.

VI. SIMULATION RESULTS

Simulation results are provided to evaluate the performance of the uplink ISAC systems. We assume 4-QAM modulation for uplink communication, and the radar waveform is assumed to be orthogonal. Unless stated otherwise, we set the simulation parameters as follows. The numbers of the antennas equipped at the transmitter, receiver, and the number of the CUs are set to $M_t = 4$, $N_r = 8$, and $K = 8$, respectively. To better show the performance gap of different receivers, the prior information of the target response is not exploited and we assume that $L = 16$ snapshots are jointly processed. The communication channel is generated following the distribution of $\mathrm{vec}(\mathbf{H}_c) \sim \mathcal{CN}(\mathbf{0}, \mathbf{I}_K)$. It is assumed that the normalized transmit power of the communication signal is $P_c = 1$ W, while the noise power is set to $\sigma^2 = -20$ dBw. The penalty parameter is initialized as $\mu_0 = 0.001$, with a standard step size in the subgradient method and the update rule presented in [32]. The tradeoff factor in each iteration is updated as $\rho_l = 0.05^l$. The maximum iteration times for the outer and inner layers are set as $l_{\max} = 200$, $k_{\max} = 100$, respectively. We use the homotopy optimization method outlined in subsection IV-B for the SIC-type, projection-type, and FP-type receivers, with parameters set the same as those for the DFP-type receivers.

A. Performance Comparison of the Proposed Receivers

In this subsection, we evaluate the S&C performance of the proposed algorithm, as shown in Fig. 6 and Fig. 7. In Fig. 6, we examine the BER of different types of receivers under different signal-to-interference ratio (SIR) of the communication signal detection problem $\mathrm{SIR} \triangleq P_c/P_r$. As observed in Fig. 6, the
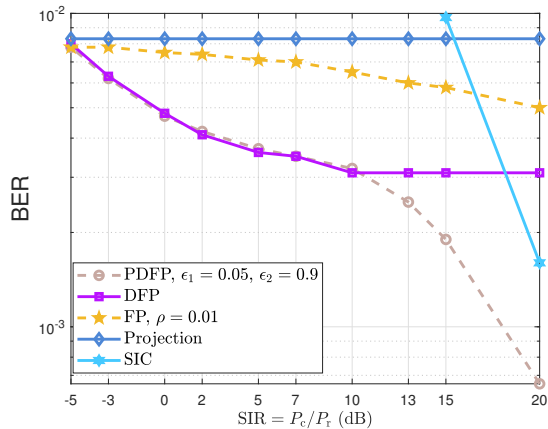
Fig. 6: BER of different types of receivers

Fig. 7: NMSE versus the sensing SNR

projection-type receivers exhibit a constant BER across different SIR levels, indicating a lack of environmental adaptation. The performance of the SIC-type receivers deteriorates when the SIR is below 15 dB, suggesting that they are only effective when the sensing signal is weak. In contrast, the proposed DFP-type receivers outperform both the projection-type and FP-type receivers, especially at higher SIR levels. However, their performance begins to saturate when the SIR exceeds 10 dB. The PDFP-type receivers, which combine two DFP-type receivers to enhance environmental adaptation, provide improved performance across a wider range of SIR values.

In Fig. 7, we examine the normalized mean square error (NMSE) of the target response vector $\mathbf{h}_r$ with different types of receivers as the transmit power of the sensing signal varies. The sensing SNR, corresponding to the target response estimation problem, is defined as $\mathrm{SNR_s} \triangleq P_r/\sigma^2$. It can be observed that the NMSE of the projection-type receivers and the DFP receivers decreases as the transmit power increases, less than 0.02 when $\mathrm{SNR_s} = 20$ dB. Besides, DFP-type receivers have better performance than the FP-type receivers as they address the communication signal detection task more efficiently. However, the performance of the SIC-type receivers does not improve monotonically as the sensing SNR increases. This is because, in the SIC-type receivers, the communication signal detection performance in the first stage is poor when the transmit power of the sensing signal is high. In this case, the residual communication signal detection error is much larger than the noise, which degrades the subsequent sensing performance. Therefore, projection-type receivers and the proposed DFP-type receivers, are better suited to achieve desired S&C performance simultaneously.

B. Impact of System Parameters

In Fig. 8, we evaluate the performance of different types of receivers under different noise densities. The SNR of the signal detection problem is defined as $\mathrm{SNR_c} \triangleq P_c/\sigma^2$. In Fig. 8(a), we consider the typical i.i.d. Gaussian channel, while in Fig. 8(b), we consider a correlated communication channel with a correlation coefficient of $r = 0.3$ [37]. It can be observed that adopting the DFP-type receivers yields better performance than the projection-type receivers using the homotopy optimization, and approaches the performance of
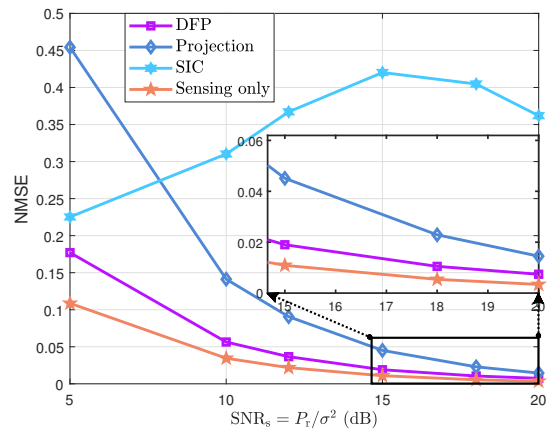
the projection-type receivers using the SDR detector. However, the computational complexity of SDR is approximately 100 times higher than that of the DFP-type receivers using the homotopy optimization, with a complexity of $\mathcal{O}\left(L^{3.5}K^{3.5}\right)$. Furthermore, compared to $P_r = 0$ dBw, $P_r = -5$ dBw provides better signal detection performance, especially when $\mathrm{SNR_c}$ is large. This can be interpreted as a S&C performance tradeoff by varying the transmit power. Finally, the performance of the uplink ISAC receivers deteriorates when the communication channels are correlated, but the performance trend remains similar.

In Fig. 9, we evaluate the impact of increasing the number of antennas under different system setups. We assume $P_r = 1$ W and consider a critically determined communication channel, i.e., $K = M_r$. The results show that the number of snapshots significantly affects the decoder's performance. When the number of snapshots is fixed at $L = 16$, increasing the number of antennas provides limited performance gain. However, when the number of snapshots increases with the number of antennas, i.e., $L = M_t + 8$, the BER decreases rapidly as the number of antennas increases, similar to the trend observed in MIMO communication systems [15]. When $K = M_r = 40$ and $\sigma^2 = -20$ dB, the BER approaches 10^{-7}, much smaller than in the case with fixed snapshots. This suggests that the number of snapshots should scale with the number of antennas to fully harness the potential of uplink ISAC systems. Furthermore, it is observed that increasing the number of transmit antennas for sensing can lead to an increase in BER due to the rank deficiency issue, as discussed in Lemma 1.

C. Employing Block Structure in the Receivers

In Fig. 10, we examine the benefits of applying a block structure in uplink ISAC receivers. Each sub-block contains 20 snapshots, and the PDFP-type receivers are considered. The NMSE of the target response vector estimation and the BER are shown in Fig. 10(a) and Fig. 10(b), respectively, with varying numbers of snapshots (or equivalently, the number of sub blocks). It can be observed that as the number of snapshots increases, both the NMSE and the BER decrease. The decrease in BER can be explained as follows: increasing the number of snapshots improves the target response estimation
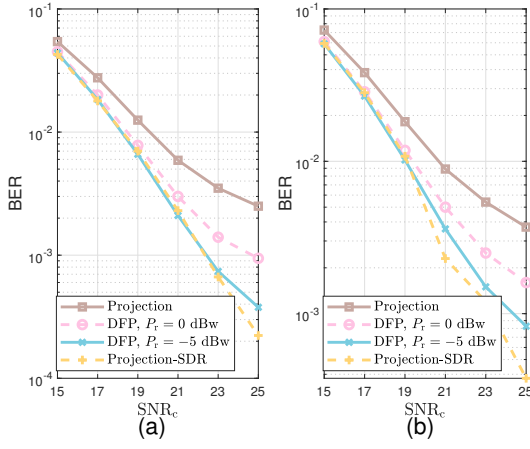
Fig. 8: BER of different types of receivers versus communication SNR under Gaussian channel (a) and correlated channel (b)
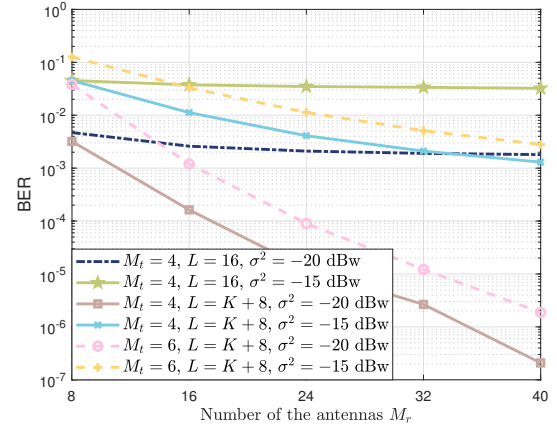

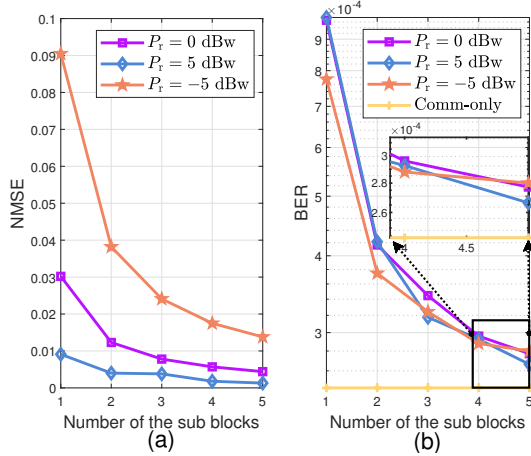Fig. 9: BER under different systems setup

Fig. 10: S&C performance of versus the number of the sub blocks

precision, and a more accurate approximation of the target response reduces radar signal interference, leading to better communication performance. Additionally, when the number of sub-blocks is small, higher sensing signal power improves target response estimation but also increases BER. However, as the number of sub blocks increases, the NMSE and radar signal interference become negligible, allowing the BER of the uplink ISAC systems with varying sensing signal power to approach that of the communication only systems.

VII. CONCLUSION

In this paper, the joint signal detection and target response estimation problem in uplink ISAC systems was investigated, and a general receiver framework termed FP-type receivers with a tradeoff factor was introduced. In the FP-type receivers, communication signals were detected using a reconstructed signal. It was shown that decreasing the tradeoff factor improved the SINR of the signal detection problem but also amplified the undesired correlation between the reconstructed signal. The PEP of the FP-type receivers under both ML and ZF detectors was studied, revealing that the optimal tradeoff factor depends not only on the communication signal detection algorithm but also on the environment. Building on a MIMO signal detection algorithm using homotopy optimization, DFP-type receivers were proposed, transforming the signal de-

tection problem into a continuous optimization problem. By adjusting the tradeoff factor in each iteration, DFP-type receivers provided smoother approximations to the original problem and offered improved environmental adaptability. Two extensions were then discussed: PDFP-type receivers, which used multiple DFP-type receivers for enhanced environmental adaptability, and the block structure of uplink ISAC receivers, which incorporated prior target information to further enhance performance.

APPENDIX A
PROOF FOR THEOREM 1

The SINR of the transformed signal detection problem using the FP-type receivers is given by

$$
\begin{aligned}
\text{SINR}_{\text{FP}} &\triangleq \frac{\mathbb{E}\left[\|\mathbf{\Gamma}_{\text{T}}\mathbf{A}_{\text{c}}\mathbf{x}_{\text{c}}\|_2^2\right]}{\mathbb{E}\left[\|\mathbf{\Gamma}_{\text{T}}\mathbf{A}_{\text{r}}\mathbf{h}_{\text{r}}\|_2^2\right] + \mathbb{E}\left[\|\mathbf{\Gamma}_{\text{T}}\mathbf{n}\|_2^2\right]} \\
&= \frac{\mathbb{E}\left[\|\mathbf{\Gamma}_{\text{T}}\mathbf{A}_{\text{c}}\mathbf{x}_{\text{c}}\|_2^2\right]}{\rho^2\mathbb{E}\left[\|\mathbf{A}_{\text{r}}\mathbf{h}_{\text{r}}\|_2^2\right] + \mathbb{E}\left[\|\mathbf{\Gamma}_{\text{T}}\mathbf{n}\|_2^2\right]}, \\
&= \frac{\mathbb{E}\left[\text{Tr}(\mathbf{\Gamma}_{\text{FP}}\mathbf{A}_{\text{c}}\mathbb{E}\left[\mathbf{x}_{\text{c}}\mathbf{x}_{\text{c}}^{\text{H}}\right]\mathbf{A}_{\text{c}}^{\text{H}}\mathbf{\Gamma}_{\text{FP}}^{\text{H}})\right]}{\rho^2\mathbb{E}\left[\|\mathbf{H}_{\text{r}}\mathbf{X}_{\text{r}}\|_F^2\right] + \text{Tr}(\mathbf{\Gamma}_{\text{FP}}\mathbb{E}\left[\mathbf{n}\mathbf{n}^{\text{H}}\right]\mathbf{\Gamma}_{\text{FP}}^{\text{H}})} \\
&\overset{(a)}{=} \frac{P_{\text{c}}\mathbb{E}\left[\text{Tr}(\mathbf{G}_{\text{FP}}\mathbf{G}_{\text{FP}}^{\text{H}})\right]}{\rho^2 L P_{\text{s}} + \text{Tr}(\mathbf{\Gamma}_{\text{FP}}\mathbf{\Gamma}_{\text{FP}}^{\text{H}})K\sigma^2},
\end{aligned} \tag{A.1}
$$

where (a) exploits the distribution of the uplink communication signal. Then, we have

$$
\begin{aligned}
(A.1) &= \frac{P_{\text{c}}\mathbb{E}\left[\text{Tr}(\mathbf{G}_{\text{FP}}\mathbf{G}_{\text{FP}}^{\text{H}})\right]}{\rho^2 L P_{\text{s}} + \text{Tr}(\mathbf{\Gamma}_{\text{FP}}\mathbf{\Gamma}_{\text{FP}}^{\text{H}})K\sigma^2} \\
&= \frac{P_{\text{c}}\mathbb{E}\left[\text{Tr}(\mathbf{P}_{\text{FP}}\mathbf{P}_{\text{FP}}^{\text{H}} \otimes \mathbf{H}_{\text{c}}\mathbf{H}_{\text{c}}^{\text{H}})\right]}{\rho^2 L P_{\text{s}} + \text{Tr}(\mathbf{P}_{\text{FP}}\mathbf{P}_{\text{FP}}^{\text{H}} \otimes \mathbf{I}_{M_r})K\sigma^2} \\
&= \frac{P_{\text{c}}\,\text{Tr}(\mathbf{P}_{\text{FP}}\mathbf{P}_{\text{FP}}^{\text{H}})\mathbb{E}\left[\text{Tr}(\mathbf{H}_{\text{c}}\mathbf{H}_{\text{c}}^{\text{H}})\right]}{\rho^2 L P_{\text{s}} + \text{Tr}(\mathbf{P}_{\text{FP}}\mathbf{P}_{\text{FP}}^{\text{H}})\,\text{Tr}(\mathbf{I}_{M_r})K\sigma^2} \\
&= \frac{P_{\text{c}}((1-\rho^2)\,\text{Tr}(\mathbf{P}_{\perp}) + \rho^2\,\text{Tr}(\mathbf{I}_L))KM_r}{\rho^2 L P_{\text{s}} + ((1-\rho^2)\,\text{Tr}(\mathbf{P}_{\perp}) + \rho^2\,\text{Tr}(\mathbf{I}_L))M_rK\sigma^2} \\
&= \frac{P_{\text{c}}(L - (1-\rho^2)M_t)KM_r}{\rho^2 L P_{\text{s}} + (L - (1-\rho^2)M_t)M_rK\sigma^2}.
\end{aligned} \tag{A.2}
$$

It can be easily observed that the SINR_{FP} is an decreasing function w.r.t. $g(\rho^2) = L\rho^2/(L - (1-\rho^2)M_t), \rho^2 \in$

$[0, 1], L \geq M_t$. By deriving the first order partial derivation of $\frac{\partial g}{\partial \rho^2}$, we have

$$\frac{\partial g}{\partial \rho^2} = \frac{L - M_t}{\left(L - (1 - \rho^2)M_t\right)^2} > 0. \tag{A.3}$$

Therefore, SINR_{FP} is an decreasing function w.r.t. ρ.

APPENDIX B
PROOF FOR LEMMA 4

Lemma 4 can be proved by combining Theorem 1 and Theorem 2. Since we have

$$\overline{\mathbf{G}}^{\text{T}}(\rho)\overline{\mathbf{G}}(\rho) = \begin{bmatrix} \mathbf{G}_{\text{FP}}^{\text{H}}\mathbf{G}_{\text{FP}} & \mathbf{0} \\ \mathbf{0} & \mathbf{G}_{\text{FP}}^{\text{H}}\mathbf{G}_{\text{FP}} \end{bmatrix} \tag{B.1}$$

and $\lambda_1(\mathbf{P}_{\text{FP}}^{\text{H}}\mathbf{P}_{\text{FP}}) = 1$. The largest eigenvalue of matrix $\overline{\mathbf{G}}^{\text{T}}(\rho)\overline{\mathbf{G}}(\rho)$ is given by

$$\lambda_1(\overline{\mathbf{G}}^{\text{T}}(\rho)\overline{\mathbf{G}}(\rho)) = \lambda_1(\mathbf{G}_{\text{FP}}^{\text{H}}\mathbf{G}_{\text{FP}}) \tag{B.2}$$
$$= \lambda_1(\mathbf{P}_{\text{FP}}^{\text{H}}\mathbf{P}_{\text{FP}})\lambda_1(\mathbf{H}_{\text{c}}^{\text{H}}\mathbf{H}_{\text{c}}) = \lambda_1(\mathbf{H}_{\text{c}}^{\text{H}}\mathbf{H}_{\text{c}}).$$

According to Theorem 2, it can be proved that Problem (35) is equivalent to the transformed signal detection problem in (30). Finally, when $\rho = 0$, the FP-type receivers reduce to the conventional projection-type receivers, thereby achieving the equivalence between the transformed signal detection problem and the original ML estimation problem in (4).

REFERENCES

[1] S. Lu, F. Liu, Y. Li, K. Zhang, H. Huang, J. Zou, X. Li, Y. Dong, F. Dong, J. Zhu, Y. Xiong, W. Yuan, Y. Cui, and L. Hanzo, "Integrated sensing and communications: Recent advances and ten open challenges," *IEEE Internet Things J.*, vol. 11, no. 11, pp. 19 094–19 120, Jun. 2024.

[2] F. Liu, W. Yuan, C. Masouros, and J. Yuan, "Radar-assisted predictive beamforming for vehicular links: Communication served by sensing," *IEEE Trans. Wireless Commun.*, vol. 19, no. 11, pp. 7704–7719, Nov. 2020.

[3] Y. Song, Y. Zeng, Y. Yang, Z. Ren, G. Cheng, X. Xu, J. Xu, S. Jin, and R. Zhang, "An overview of cellular ISAC for low-altitude UAV: New opportunities and challenges." [Online]. Available: https://arxiv.org/abs/2412.19973

[4] J. Tang, Y. Yu, C. Pan, H. Ren, D. Wang, J. Wang, and X. You, "Cooperative ISAC-empowered low-altitude economys." [Online]. Available: https://arxiv.org/abs/2412.20371

[5] F. Liu, C. Masouros, A. P. Petropulu, H. Griffiths, and L. Hanzo, "Joint radar and communication design: Applications, state-of-the-art, and the road ahead," *IEEE Trans. Commun.*, vol. 68, no. 6, pp. 3834–3862, Jun. 2020.

[6] M. Temiz, E. Alsusa, and M. W. Baidas, "A dual-function massive MIMO uplink OFDM communication and radar architecture," *IEEE Trans. Cognit. Commun. Netw.*, vol. 8, no. 2, pp. 750–762, Jun. 2022.

[7] C. Ouyang, Y. Liu, and H. Yang, "Performance of downlink and uplink integrated sensing and communications (ISAC) systems," *IEEE Wireless Commun. Lett.*, vol. 11, no. 9, pp. 1850–1854, Sep. 2022.

[8] ——, "Revealing the impact of SIC in NOMA-ISAC," *IEEE Wireless Commun. Lett.*, vol. 12, no. 10, pp. 1707–1711, Oct. 2023.

[9] B. Zhao, C. Ouyang, X. Zhang, and Y. Liu, "Downlink and uplink NOMA-ISAC with signal alignment," *IEEE Trans. Wireless Commun.*, vol. 23, no. 10, pp. 15 322–15 338, Oct. 2024.

[10] L. Sun, Z. Zhao, S. Wang, Z. Ding, and M. Peng, "On the study of non-orthogonal multiple access (NOMA)-assisted integrated sensing and communication (ISAC)," *IEEE Trans. Commun.*, vol. 72, no. 11, pp. 7278–7293, Nov. 2024.

[11] Q. Qi, X. Chen, C. Zhong, C. Yuen, and Z. Zhang, "Deep learning-based design of uplink integrated sensing and communication," *IEEE Trans. Wireless Commun.*, vol. 23, no. 9, pp. 10 639–10 652, Sep. 2024.

[12] Z. He, W. Xu, H. Shen, D. W. K. Ng, Y. C. Eldar, and X. You, "Full-duplex communication for ISAC: Joint beamforming and power optimization," *IEEE J. Select. Areas Commun.*, vol. 41, no. 9, pp. 2920–2936, Sep. 2023.

[13] R. Li, L. Wang, K. Chen, L. Xu, and A. Fei, "Full-duplex NOMA-enabled integrated sensing and communication: Joint transmit and receive beamforming optimization," *IEEE Internet Things J.*, vol. 11, no. 16, pp. 27 015–27 029, Aug. 2024.

[14] Y. Dong, F. Liu, and Y. Xiong, "Joint receiver design for integrated sensing and communications," *IEEE Commun. Lett.*, vol. 27, no. 7, pp. 1854–1858, Jul. 2023.

[15] H. He, C.-K. Wen, S. Jin, and G. Y. Li, "Model-driven deep learning for MIMO detection," *IEEE Trans. Signal Process.*, vol. 68, pp. 1702–1715, 2020.

[16] L. Zheng, M. Lops, and X. Wang, "Adaptive interference removal for uncoordinated radar/communication coexistence," *IEEE J. Sel. Top. Sign. Proces.*, vol. 12, no. 1, pp. 45–60, Feb. 2018.

[17] J. Johnston, Y. Li, M. Lops, and X. Wang, "ADMM-net for communication interference removal in stepped-frequency radar," *IEEE Trans. Signal Process.*, vol. 69, pp. 2818–2832, Apr. 2021.

[18] Z. Yu, H. Ren, C. Pan, G. Zhou, R. Wang, M. Liu, and J. Wang, "Addressing the mutual interference in uplink ISAC receivers: A projection method," *IEEE Wireless Commun. Lett.*, vol. 13, no. 11, pp. 3109–3113, Nov. 2024.

[19] J. A. Zhang, F. Liu, C. Masouros, R. W. Heath, Z. Feng, L. Zheng, and A. Petropulu, "An overview of signal processing techniques for joint communication and radar sensing," *IEEE J. Sel. Top. Sign. Proces.*, vol. 15, no. 6, pp. 1295–1315, Nov. 2021.

[20] X.-D. Zhang, *Matrix analysis and applications*. Cambridge University Press, 2017.

[21] A. Liao, Z. Bai, and Y. Lei, "Best approximate solution of matrix equation AXB + CYD = E," *SIAM Journal on Matrix Analysis and Applications*, vol. 27, no. 3, pp. 675–688, 2005.

[22] J. G. Proakis and M. Salehi, *Digital Communications*, 5th ed. New York, NY: McGraw-Hill, 2008.

[23] L. Lu, G. Y. Li, A. L. Swindlehurst, A. Ashikhmin, and R. Zhang, "An overview of massive MIMO: Benefits and challenges," *IEEE J. Sel. Top. Sign. Proces.*, vol. 8, no. 5, pp. 742–758, Oct. 2014.

[24] E. Biglieri, G. Taricco, and A. Tulino, "Performance of space-time codes for a large number of antennas," *IEEE Trans. Inform. Theory*, vol. 48, no. 7, pp. 1794–1803, Jul. 2002.

[25] M. Khani, M. Alizadeh, J. Hoydis, and P. Fleming, "Adaptive neural signal detection for massive MIMO," *IEEE Trans. Wireless Commun.*, vol. 19, no. 8, pp. 5635–5648, Aug. 2020.

[26] L. Liu, C. Yuen, Y. L. Guan, Y. Li, and Y. Su, "Convergence analysis and assurance for gaussian message passing iterative detector in massive MU-MIMO systems," *IEEE Trans. Wireless Commun.*, vol. 15, no. 9, pp. 6487–6501, Jun. 2016.

[27] Z. Wang, R. M. Gower, Y. Xia, L. He, and Y. Huang, "Randomized iterative methods for low-complexity large-scale MIMO detection," *IEEE Trans. Signal Process.*, vol. 70, pp. 2934–2949, 2022.

[28] K.-K. Wong, A. Paulraj, and R. D. Murch, "Efficient high-performance decoding for overloaded MIMO antenna systems," *IEEE Trans. Wireless Commun.*, vol. 6, no. 5, pp. 1833–1843, May 2007.

[29] W.-K. Ma, C.-C. Su, J. Jalden, T.-H. Chang, and C.-Y. Chi, "The equivalence of semidefinite relaxation MIMO detectors for higher-order QAM," *IEEE J. Sel. Top. Sign. Proces.*, vol. 3, no. 6, pp. 1038–1052, Dec. 2009.

[30] D. M. Dunlavy and D. P. O'Leary, "Homotopy optimization methods for global optimization." Sandia National Laboratories (SNL), Albuquerque, NM, and Livermore, CA, Tech. Rep., 2005.

[31] M. Shao and W.-K. Ma, "Binary MIMO detection via homotopy optimization and its deep adaptation," *IEEE Trans. Signal Process.*, vol. 69, pp. 781–796, 2021.

[32] J. Liu, Y. Liu, W.-K. Ma, M. Shao, and A. M.-C. So, "Extreme point pursuit—part I: A framework for constant modulus optimization," *IEEE Trans. Signal Process.*, early access, 2024.

[33] R. T. Rockafellar, *Convex Analysis*. Princeton University Press, 1970.

[34] A. Beck, *First-order methods in optimization*. SIAM, 2017.

[35] L. He, Z. Wang, S. Yang, T. Liu, and Y. Huang, "Generalizing projected gradient descent for deep-learning-aided massive MIMO detection," *IEEE Trans. Wireless Commun.*, vol. 23, no. 3, pp. 1827–1839, Mar. 2024.

[36] M. Shao, Q. Li, W.-K. Ma, and A. M.-C. So, "A framework for one-bit and constant-envelope precoding over multiuser massive MISO channels," *IEEE Trans. Signal Process.*, vol. 67, no. 20, pp. 5309–5324, Oct. 2019.

[37] S. Loyka, "Channel capacity of MIMO architecture using the exponential correlation matrix," *IEEE Commun. Lett.*, vol. 5, no. 9, pp. 369–371, Sep. 2001.